Astron. Astrophys. 344, 935–941 (1999)

ASTRONOMY AND ASTROPHYSICS

Turbulence variation in the atmosphere of δ Cephei

D. Gillet[1], **A.B. Fokin**[2], **M.G. Breitfellner**[3], **S. Mazauric**[1], **and A. Nicolas**[4]

[1] Observatoire de Haute-Provence – CNRS, F-04870 Saint-Michel l'Observatoire, France
[2] Institute for Astronomy of the Russia Academy of Sciences, 48 Pjatnitskaja, 109017 Moscow, Russia
[3] ESA Villafranca Del Castillo, ISO Science Team, Apartado – P.O. Box 50727, E-28080 Madrid, Spain
[4] Ecole Normale Supérieure de Lyon, 46 allée d'Italie, F-69364 Lyon Cedex 07, France

Received 16 July 1998 / Accepted 18 January 1999

Abstract. Using 288 high resolution spectra obtained over 3 consecutive years (1993–1995), the microturbulence velocity curve of δ Cephei is determined with a high temporal resolution. From the observed FWHM variation of the unblended Fe I 5576.0883 Å absorption line, and from nonlinear nonadiabatic pulsating models, it is shown that the global compression/expansion of the atmosphere provokes the variation of the turbulence. The turbulent velocity reaches its maximum, of about $7\,\mathrm{km\,s^{-1}}$, at minimum radius, and decreases up to $2\,\mathrm{km\,s^{-1}}$ during the expansion of the star. It is also shown that the compression waves and shocks certainly provoke some rapid turbulence variations during their propagation in the atmosphere. The turbulence amplification due to these waves, being in general smaller than the global compression effect, increases with the wave amplitude.

Key words: line: profiles – shock waves – turbulence – stars: individual: δ Cep – stars: variables: Cepheids

1. Introduction

Among the radial variable stars, the classical Cepheids are the best known. They are recognized not only as primary Galactic and extragalactic distance indicators but also as standard objects to study the physical mechanisms which govern their pulsation as well as the supersonic phenomena occurring within their extended atmosphere. During the last ten years, several important open questions have been investigated both theoretically and observationally (see the recent reviews of Bono et al. 1998 and Buchler 1998). In particular, current pulsational models are sophisticated enough to study in detail the complexe dynamics of the atmospheres of these stars and to compare the theoretical line profiles with high resolution observations. Moreover, models containing a nonlocal and time-dependent treatment of stellar convection are now proposed to study the effects of convection on pulsation via nonlinear (Bono et al. 1998 for classical Cepheids) or linear (Xiong et al. 1998 for RR Lyrae stars) nonadiabatic analysis. Thus, we can expect that in the near future the structure of the turbulent atmospheres of pulsating stars would be better investigated.

Recently Fokin, Gillet & Breitfellner (1996, hereafter FGB) showed that the velocity field in the atmosphere of a pulsating star (δ Cephei) is an important line broadening source. It is thus imperative to take into account the high amplitude compression waves and shock waves propagating in this type of atmosphere to evaluate line profiles and physical quantities which can be deduced from them, such as the turbulence velocity.

Breitfellner & Gillet (1993) in their early determination of the turbulence curve did not consider the effect of the velocity gradient. Consequently, they obtain an overestimation of the turbulence velocity with a maximum around $13\,\mathrm{km\,s^{-1}}$ and a minimum value of $7.5\,\mathrm{km\,s^{-1}}$. Their turbulence curve presents three obvious peaks. The main one occurs around the maximum compression, a moderate peak is visible around phase $\varphi = 0.6$ and a smaller one is present at phase 0.1 after the maximum compression ($\varphi = 0.9$). The main peak is broadened on its left side (phase interval 0.75–0.80).

Contrary to Breitfellner & Gillet (1993), FGB do not limit the determination of the turbulence velocity to one line parameter (i.e. the Full Width at Half Maximum) but they use the whole line profile. Nevertheless, as noted by FGB, this method is difficult to apply because presently nonlinear models are not sufficiently adequate. Some model factors, which remain sometimes uncertain, can affect the calculated line profile, for example, rotation, chemical composition, non-LTE effects, low-temperature mean opacity and radiative cooling rate etc. Consequently, it is difficult to estimate the relevant turbulent velocity v_{turb} from a detailed comparison of the calculated and observed line profiles. However, the FWHM of an absorption line is a less sensitive parameter with respect to these factors. In particular, its value seems to be weakly affected by non-LTE effects or temperature variations. For this reason it seems more preferable to limit the determination of the turbulence velocity to this single parameter. The use of the residual flux or the equivalent width does not seem actually appropriate for quantitative estimation of v_{turb}.

The idea that the main peak observed in the width of absorption lines is due to the turbulent convective velocity field has been first suggested by Benz and Stellingwerf (1985) for RR Lyrae. Chadid and Gillet (1997) have put into evidence that this peak is essentially caused by the line doubling provoked

by the propagation of a shock wave. This result has been recently confirmed by a theoretical approach (Fokin et al. 1998). Bono et al. (1998), using a nonlocal and time-dependent treatment of stellar convection, suggest that turbulent convection can contribute to the broadening of absorption lines observed in classical Cepheids. By comparing the convective velocity perturbations close to the photospheric layers with the microturbulence velocities obtained by spectroscopic measurements, they find that the convective velocity and its variation over the pulsation cycle reasonably agree with observations except for models located close to the blue edge. Nevertheless, due to the poor spatial resolution of their models in the outermost layers for continuum optical depths larger than 0.05, Bono et al. cannot take into account in detail the effects of velocity gradients induced by the presence of compression and shock waves. Moreover, their calculations show that the convective turbulent velocity is either vanishing or attain very low values at low optical depths, where the observed absorption lines are formed. Consequently, because the convective energy transport becomes negligible in the line formation layers, it is not clear that convective turbulent velocities and microturbulent velocities obtained by spectroscopic measurements are directly correlated.

Recently, Gillet et al. (1998) have discussed the turbulence amplification in the atmosphere of pulsating stars. In particular, it is shown that the turbulence variation is not only due to the global compression of the atmosphere during the pulsation. Indeed, strong shock waves propagating from the deep photosphere to high atmospheric layers can also play a role in the turbulence amplification. Because the presence of these waves are predicted by nonlinear nonadiabatic models (for instance FGB), it is interesting to look for their observational signatures. The analysis of the shape of spectral lines with high resolution spectrographs are well adapted if the temporal resolution of observations is large enough because the effects induced by the shock passage in the line formation region are rapid. The main goal of this study is to obtain, for the first time, this kind of observations, and then to try to detect if the turbulence amplification due to shocks is, or is not present. In their previous paper, FGB use a too poor temporal resolution to reach this objective.

In this paper we estimate the FWHM curve and evaluate the variation of v_{turb} for the variable star δ Cephei, using high-resolution spectra obtained during 3 years. For the moment, this data compilation is the most complete and precise one. Sect. 2 presents observations. In Sect. 3, we describe the variation of the main line parameters, with a qualitative interpretation in the framework of the nonlinear nonadiabatic models. The turbulence velocity curve is discussed in Sect. 4, and some The turbulence velocity curve is discussed in Sect. 4, and some concluding remarks are given in Sect. 5.

2. Observations

As in our previous work (Breitfellner & Gillet 1993), we have selected in the spectrum of the classical Cepheid star δ Cephei the unblended Fe I 5576.0883 Å absorption line. The observations were done at the 1.52 m telescope of the Observatoire de Haute-Provence in September 8–20, 1993 (59 spectra), September 15–28, 1994 (65 spectra), from August 22 to September 4, 1995 (125 spectra) and from September 28 to October 2, 1995 (59 spectra) with the spectrograph AURELIE (Gillet et al. 1994). The high-resolution configuration of the spectrograph was the same as in FGB. The dispersion was of 3.23 Å mm^{-1} (0.042 Å pixel^{-1} or 2.26 km s^{-1} pixel^{-1}) and led to a resolution of 0.113 Å (6.1 km s^{-1}, $R \equiv \lambda/\Delta\lambda \simeq 49\,000$). Integration times were between several minutes and half an hour, depending on the magnitude of δ Cephei (between 3.5 and 4.5) and the weather conditions, giving a signal-to-noise ratio around 400 ± 100 at the continuum level. The data reduction processing is described in Breitfellner & Gillet (1993) and we have used the same ephemeris to compute the pulsational phases.

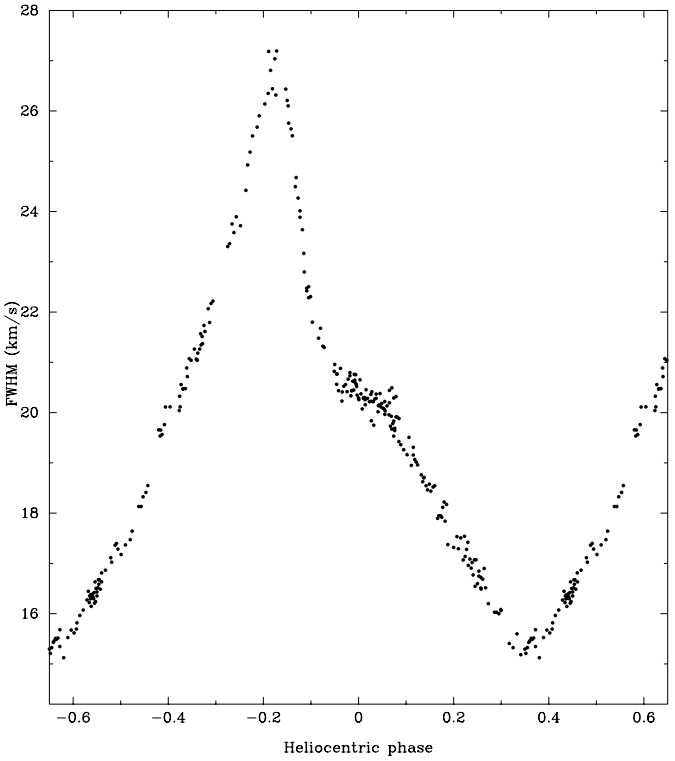

Fig. 1. Variation of the FWHM of the unblended Fe I 5576.0883 Å absorption line of δ Cephei. The 288 spectra were obtained over 3 years, from September 1993 to October 1995. The sample standard deviation is 0.21 km s^{-1}

Finally, 288 FWHM have been measured between pulsation cycle number 1208 and 1438 i.e., over an interval of 230 cycles (with the period of 5.4 days). These results are shown in Fig. 1. Although δ Cephei is known to have rather stable velocity curve (in shape and amplitude) over about a century (Butler 1993), some weak dispersion of points exists due to not very strict repetition of cycles. An analysis of the distribution of FWHM measures shows that the scattering is approximately the same at all phases. Thus, no fine structure of the FWHM curve can be clearly detected, only a broad peak centered at phase 0.82, and a large "stillstand" around the luminosity maximum (phase 0.0) are visible.

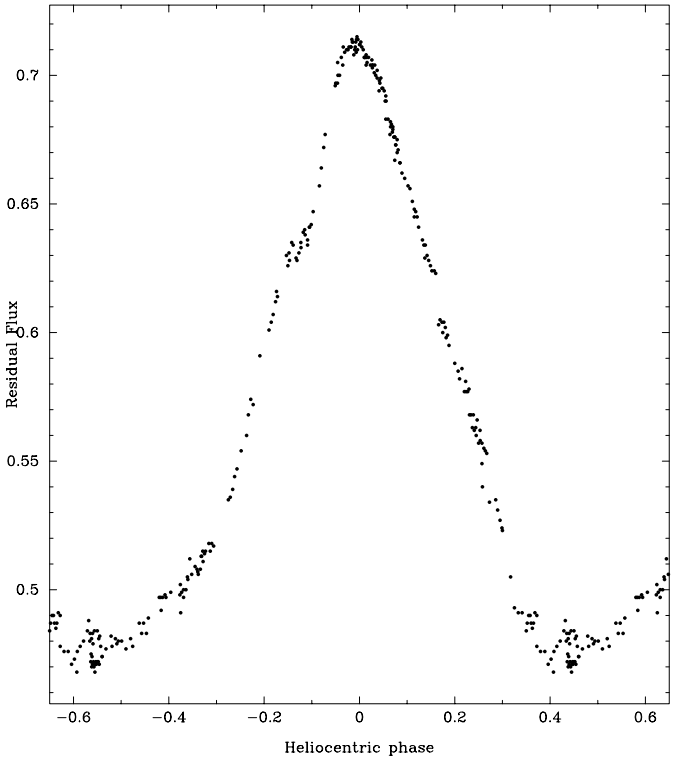

Fig. 2. Same as Fig. 1 but for the residual flux. The sample standard deviation is 0.004

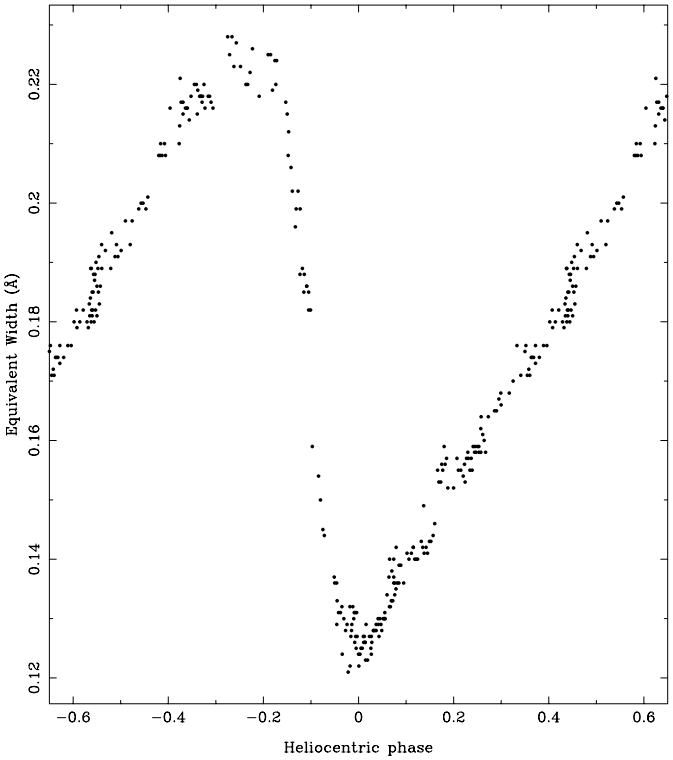

Fig. 3. Same as Fig. 1 but for the equivalent width (EW). The sample standard deviation is 0.003 Å

Figs. 2 and 3 show the residual flux (RF) and the equivalent width (EW) of the Fe I line, respectively, while (Fig. 4) gives the radial velocity curve measured with a Gaussian fit.

3. Description of the observations

One of the remarkable features of the Fe I line evolution is that the EW (Fig. 3) and the radial velocity (Fig. 4) curves have the same shape. Only the EW maximum between phases 0.74 and 0.83 is truncated with respect to that of the radial velocity curve. Similar behavior for RR Lyrae was already observed by Chadid & Gillet (1997) for the Ba II 4934.076 Å line, which was at first wrongly identified as Fe I 4934.082 Å (see Fokin & Gillet 1997). Test calculations of the line profiles with our nonlinear nonadiabatic pulsating models showed that such an unusual behaviour of these lines is due to variation in the specific conditions of excitation and ionization of the relevant species due to changes in the atmospheric conditions within the line formation region. Dependent on the characteristics of the considered atomic transition, the concentration of the line absorbers can increase when the atmosphere is expanding and cooling, and decrease when it is compressing and heating. In general, however, there is no distinct correlation between radial velocity and EW curves.

3.1. Broadening processes

The integration of the radial velocity curve of the absorption line Fe I 5576.0883 Å shows that the maximum and minimum radii

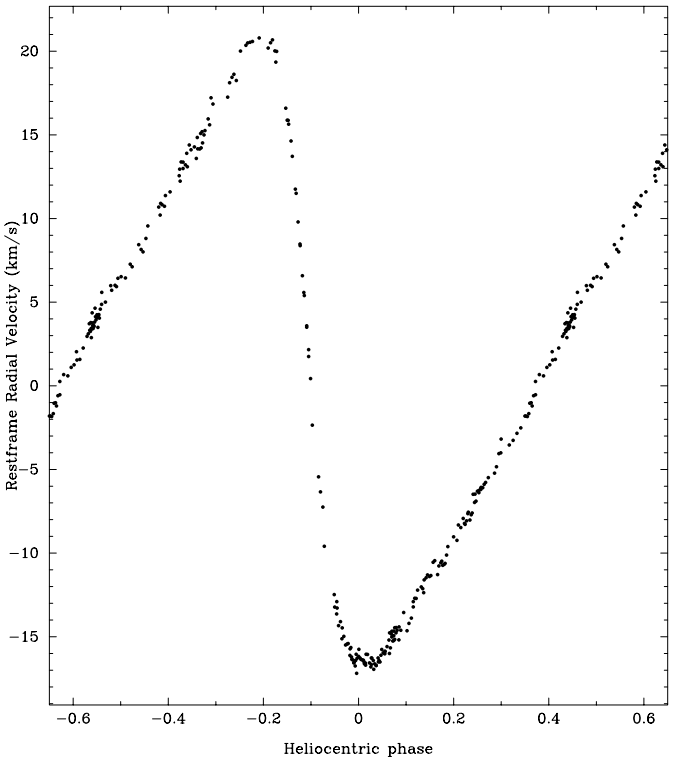

Fig. 4. Same as Fig. 1 but for the restframe radial velocity. The projection effect over the stellar disc was not taken into account. The sample standard deviation is near 0.2 km s^{-1}

occur at the pulsation phases $\varphi = 0.37$ and 0.90 respectively. The projection effect over the stellar disk is maximum in the extremes of the radial velocity, i.e., at phases 0.0 and 0.80 (Fig. 4). It is minimum when the velocity is equal to zero ($\varphi = 0.37$ and 0.90). The maxima and minima of the radial velocity gradient in the line formation region, as shown by FGB (see their Fig. 10), approximately correlate in phase with those of the projection effect. For this reason, and for the sake of simplicity, we shall refer to these both line broadening mechanisms as to general projection.

As seen from Fig. 1, the FWHM drops to its minimum value at phase 0.34, and then, during the following compression phase, constantly increases due to all main broadening mechanisms (thermal, turbulence and projection effect). For the same reason, RF and EW also increase (Fig. 5). Near phase 0.72, EW reaches its maximum value and then, from the phase 0.83, abruptly falls down to about a half of its maximum value at the minimum radius ($\varphi = 0.90$). During this phase interval, the atmospheric temperature increases and, consequently, ionizations diminish the Fe I atomic concentration. Thus, the EW decreases like observed, despite that the line remains very broad.

Even when the atmosphere begins to expand ($\varphi > 0.90$), EW still decreases until $\varphi = 0.0$. During this period, the FWHM reaches a short stillstand at about 20 km s^{-1}, because at $\varphi = 0.0$ the velocity of the expanding atmosphere is maximum and the projection effect becomes the most important for the line broadening, while the turbulence velocity decreases due to atmospheric expansion (see FGB).

When Fe I becomes more abundant, following the cooling and Fe II recombinations in the expanding atmosphere, EW starts to continuously increase, even after the atmospheric contraction begins. This is certainly the consequence of the turbulence which must be the major cause of the EW growth at the beginning of the compression phase.

FWHM reaches its maximum value near phase 0.83 before a rapid decrease (Fig. 5). This decrease must be the consequence of the fast reduction of the broadening projection effect between phases 0.83 and 0.90. After the luminosity maximum ($\varphi = 0.0$), when the projection effect begins again to decrease, FWHM constantly diminishes as well until the maximum radius ($\varphi = 0.37$). Thus, the fast variations of the projection effect appears to be at the origin of the FWHM-stillstand at $\varphi = 0.0$.

3.2. Shock wave effects?

Recently, FGB have shown that, according to nonlinear pulsation models, three main shock waves are propagating in the model atmosphere of δ Cephei during each pulsation period. These shocks pass through the Fe I line formation region (LFR) at different phases and with different intensities. The shock s1 (FGB's notation) crosses the LFR approximately in between phases 0.74 and 0.77, with maximum amplitude of $\Delta U = 16$ km s^{-1} at $\varphi = 0.77$ (see Fig. 5 of FGB), s2 between $\varphi = 0.87$ and 0.94 with $\Delta U = 19$ km s^{-1}, while s3 is visible from 0.52 to 0.54 with a maximum amplitude of 9 km s^{-1} only. Here, we adopt that a compression wave can be considered as a shock if its amplitude ΔU exceeds the sound velocity, about 8 km s^{-1}. Thus, the maximum Mach numbers of these shocks in the LFR are not larger than 2.0, 2.4 and 1.1 respectively. This means that these shocks have a relatively weak intensity in the Fe I LFR and, consequently, we should not expect large effects on the FWHM, RF and EW curves. Indeed, during the above estimated phase intervals, no particular features can be associated to shocks s1, s2 and s3 in the FWHM curve.

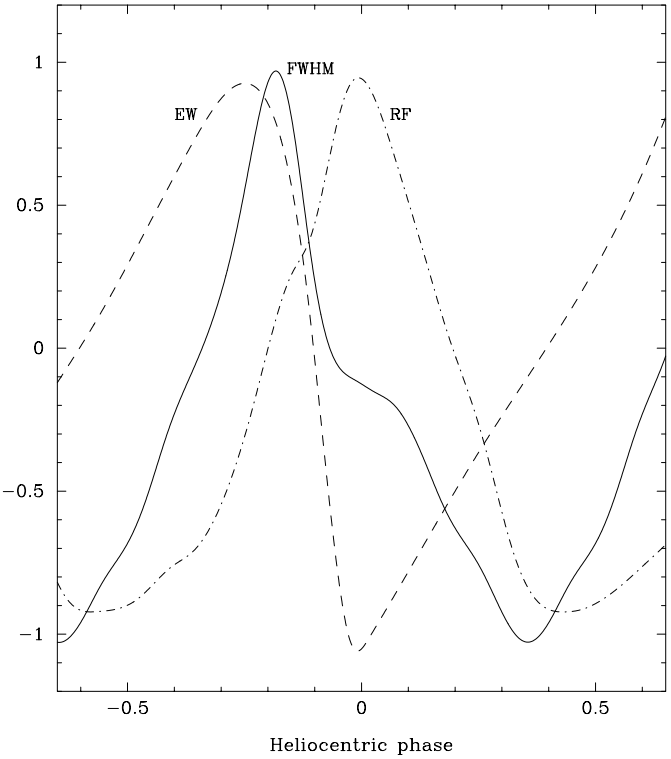

Fig. 5. Overplot of a fit of curves of Figs. 1-3. The ordinate scale is arbitrary

For the EW curve, we only remark that it begins to decrease at the same phase $\varphi = 0.74$ that s1 is expected to become a shock. We also note that the "strongest" shock s2 crosses the Fe I LFR after the minimum radius. Thus, although the atmosphere is already expanding and cooling, the transient shock heating and Fe I ionizations keep diminishing the EW, until s2 leaves the LFR. This is consistent with the fact that the observed decrease of EW ceases just after the shock s2 escapes.

In the RF curve, a short stillstand occurs somewhat between the phases 0.8 and 0.9, i.e. between the two expected passages of s1 and s2 through the LFR. We can speculate, that s1 and s2 additionally heat the gas in the LFR and thus diminish the atomic density of Fe I (increase the RF). The stillstand can be then associated with the pause between their passages. If so, this stillstand in the RF curve can be an interesting evidence of the existence of these shocks.

4. Determination of the turbulent velocity

As discussed in FGB, due to the difficulties connected with the non-LTE effects and other uncertainties in numerical modelling,

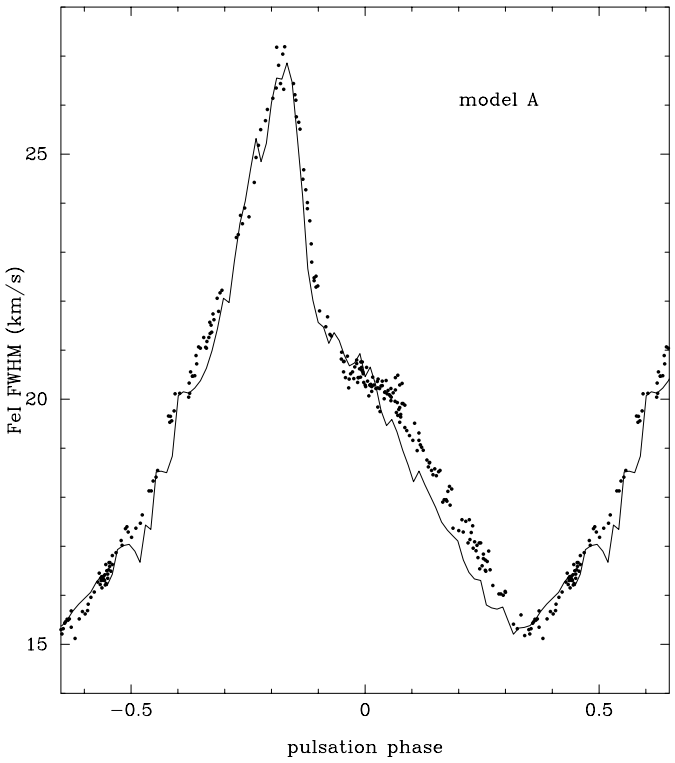

Fig. 6. Comparison between observed (points) and theoretical (solid line) FWHM of Fe I $\lambda\lambda$ 5576.0883 for δ Cephei. The calculated FWHM (model A) includes pulsation, rotation ($v_{rot} \sin i = 7.5$), velocity gradients, projection effects, and turbulence needed to fit the observed FWHM curve. The corresponding turbulent velocity is shown in Fig. 8

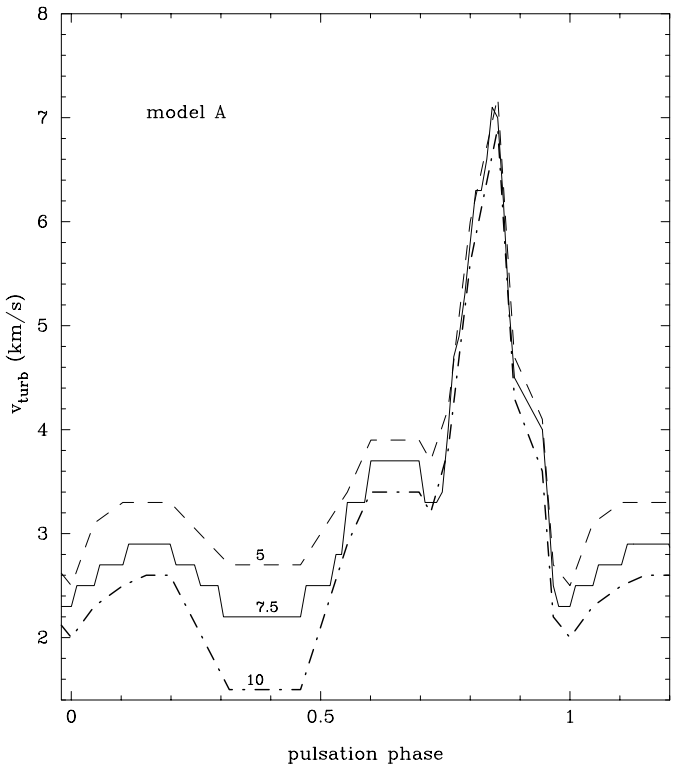

Fig. 7. Calculated turbulent velocity vs. the pulsation phase for model A for three rotational velocities $v_{rot} \sin i = 5$ (dashed), 7.5 (solid) and 10 km s^{-1} (dot-dashed).

the determination of the turbulence based on the detailed comparison of the line profiles is presently not very useful. Because the FWHM of the line does not depend much on the non-LTE effects (see FGB), it appears as the best reliable parameter to estimate the turbulent velocity. Thus, following the method developed in FGB, we have determined the turbulence velocity for three rotational velocities: $v_{rot} \sin i = 5$, 7.5 and 10 km s^{-1}. We have calculated 85 Fe I line profiles over one pulsation period to obtain a good time resolution with respect to our new observations. As in FGB, we used two nonlinear nonadiabatic pulsational models A and B, characterized by the following parameters: $T_{\rm eff} = 6056$ K, $L = 3100\,{\rm L}_\odot$, $M = 7.0\,{\rm M}_\odot$, $C_q = 1.0$, $\alpha = 0.01$, with the LAOL opacities (model A), and $T_{\rm eff} = 5750$ K, $L = 3000\,{\rm L}_\odot$, $M = 5.7\,{\rm M}_\odot$, $C_q = 1.0$, $\alpha = 0.1$, with the OP opacities (model B).

In this paper, we don't intend to evaluate in detail the dependence of the theoretical turbulent velocity on stellar parameters (M, L, T_{eff} etc.). We note, however, that although the parameters of the two selected models are quite different, we obtained similar turbulent velocity curves (see Fig. 8). So, a comparison between these models gives a good idea about sensibility to stellar parameters. The aim of our paper is not to present a quantitative survey of the effects of different parameters, but only to show a semi-quantitative general trend of v_{turb} with phase for one particular star - δ Cephei. A complete survey, which requires large additional calculations, is out of the scope of this paper. Nevertheless, this job could be a subject for a new paper.

In the line profile analysis, we included the thermal broadening mechanism, the projection effect, the stellar rotation and the pulsation velocity gradients, including those produced by the presence of the three shock waves s1, s2 and s3. Without turbulent velocity, the theoretical FWHM are lower than the observed ones, so their difference gives an estimation of the v_{turb} at each calculated phase point. Fig. 6 shows a comparison between the observed (points) and calculated (solid line) FWHM after the turbulence has been added for the model A. Similar calculation was also made for the model B. Our fit to the empirical FWHM is good enough to give an accuracy in v_{turb} between 0.3–0.5 km s^{-1}.

Fig. 7 shows the turbulent velocity for model A and for the three rotational velocities: $v_{rot} \sin i = 5$, 7.5 and 10 km s^{-1}. The rotation effect is maximum when the FWHM is minimum (phase 0.37) i.e., when the atmosphere reaches its maximum extension and has a low temperature. By contrast, when the FWHM of the line increase, especially just before the minimum radius (phase 0.85), the effect of the rotation decreases. From this calculation, we conclude that the error on the estimate of $v_{rot} \sin i$, which is some 2 km s^{-1}, does not affect the general shape of the turbulent velocity curve. In particular, the value of the maximum turbulence velocity remains close to 7 km s^{-1} and a variation of $v_{rot} \sin i$ does not cancel the two secondary bumps at phases 0.15 and 0.65. The influence of the rotational

velocity on v_{turb} was already discussed by Breitfellner & Gillet (1993).

Fig. 8 shows the resulting turbulent velocity curves for models A and B, respectively. In addition to the main peak, centered at phase 0.84, a few secondary peaks or humps are clearly seen. The main peak is associated with the global compression of the atmosphere. At the minimum radius, the turbulence approaches the sound velocity ($\sim 8\,\mathrm{km\,s^{-1}}$). The minimum of v_{turb}, occurring around the maximum radius ($\varphi = 0.37$), is about $2\,\mathrm{km\,s^{-1}}$, which is twice larger than that deduced by FGB (based, at this phase, on only one observed profile).

Near the phase 0.9, our theoretical turbulent velocity reveals a violent oscillation with an unphysically sharp decrease (not shown on Fig. 8; this phase interval

is marked by the dashed line segment). Note that at the same phase the theoretical light curve (Fig. 1 of FGB) also shows an unrealistic sharp minimum. As shown by a detailed inspection of the pulsating model, both these results are provoked by a compression wave passing through the hydrogen ionization zone (HIZ). This is typical for radiative pulsating models, and can be eliminated by introducing convective motions (Bono, Markoni & Stellingwerf 1998). In addition, in Lagrangian codes the spatial resolution in the HIZ is too low to allow to compute correctly enough the rapid variation of the gas parameters when a shock propagates through this zone. For this reason, we removed a few points near the phase 0.9 as artefacts. Thus, we are unable to determine the turbulent velocity within this phase interval and, consequently, find out the effect of the strongest shock s2 on the turbulence, because it is crossing the Fe I LFR at this time. In the meanwhile, pure radiative energy transport and the lack of spatial resolution affect the hydrodynamical solution only during this short phase (0.89–0.94), and doesn't perturb it beyond this phase, so the solution remains quite stable.

In the model A, near the phase 0.65 a bump around $3.7\,\mathrm{km\,s^{-1}}$ appears, just before the shock s1 emerges (phase 0.74), while in the model B only a hump is present (Fig. 8). The increase of v_{turb} between phases 0.5–0.7, is correlated with the passage of s3 in the LFR. As observed in our models, s3 provokes an appreciable density growing which can be a physical reason for the turbulence increase by this phase. A small ($2.9\,\mathrm{km\,s^{-1}}$) but wide bump emerges when the "buzz waves" (weak compressive waves generated just above the hydrogen recombination front, see FGB) are observed in models A and B ($0 < \varphi < 0.3$). It should be, however, noted that our detection of the turbulence variation, occurring when shocks traverse the Fe I layer, is questionable because of the additional Doppler broadening caused by these shocks in pulsating models. Namely, if these shocks are also present in observations at the same phases, a part of the deduced turbulence can be due to an underestimation of the theoretical shock wave intensity. Also, if this latter is overestimated by the hydromodel, the real turbulence velocity can be larger than this one given by the model. For example, a small gap near the phase 0.72 in model A can be connected to the theoretical overestimation of the intensity of s1 at this phase with respect to the real one. The intensity of the same shock is smaller in the model B, so there is no such a gap in this second model (Fig. 8). This effect is, thus, model dependent and should be taken with caution.

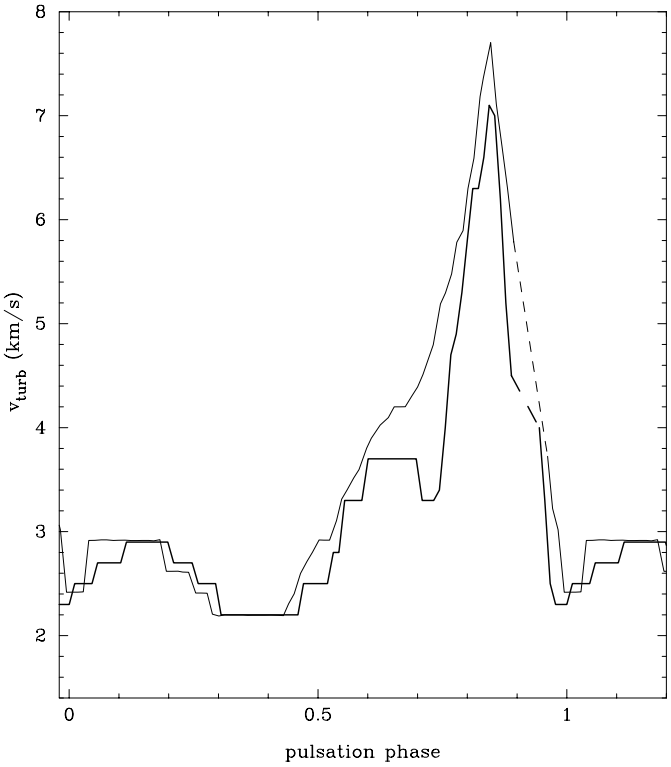

Fig. 8. Calculated turbulent velocity vs. the pulsation phase for model A (thick line) and model B (thin line), assuming a rotational velocity $v_{rot} \sin i = 7.5$. The dashed line segments indicate the phases at which numerical difficulties do not allow us to determine v_{turb}

5. Conclusions

The strongest peak in our predicted turbulent velocity curve at $\varphi = 0.85$ is certainly real, and seems associated with the global atmospheric compression. Secondary bumps at phases 0.15 and 0.65 should be taken with caution. Although they are present in both models, we cannot prove in the framework of our approach that they are real. But if they are real, then we can suggest that they are due to turbulence amplification induced by shock waves of relatively moderate intensities. In this case, the amplification should increase with the shock Mach number. It is worthwhile to note, that Sasselov & Lester (1994) have developed a completely independent pulsating atmospheric model of classical Cepheids including the chromosphere, in which they also found the shocks s1, s2 and s3.

The Lagrangean pulsation codes, such as the one used in this paper, cannot correctly resolve the hydrogen ionization zone and generates numerical artefacts. Consequently, when shocks are crossing this zone, they are certainly affected. Moreover, because the Mach number of our strongest shock (s2 occurring at phase 0.9) is relatively weak (near 2.4), it would be valuable to calculate again the turbulence curve with an adaptive code in order to increase the treatment of strong gradients and increase the accuracy of the shock front velocity.

To study the basic problem of the amplification of the turbulence by a strong shock ($M > 3$), it would be useful to perform a similar analysis of the turbulence variability for the pulsating stars in which shocks are hypersonic. With this, it would be possible to check, if the predicted turbulence amplification, based on "adiabatic" theoretical approaches (Gillet et al. 1998), are consistent or not with the observed amplification. Because strong shocks in stellar atmospheres are fully radiative, we expect that only a nonadiabatic treatment can provide realistic amplification rates.

Acknowledgements. The work of ABF has been done in part under the auspices of the CNRS (grant 97479) during a two-month stay at the Observatoire de Haute-Provence (OHP) thanks to the help of Dr. C. Bertout. ABF also aknowledges the support of the Russian Foundation for Fundamental Researches (grant 95-02-06359).

References

Benz W., Stellingwerf R.F., 1985, ApJ 297, 686
Bono G., Marconi M., Stellingwerf R.F., 1998, ApJ in press
Breitfellner M.G., Gillet D., 1993, A&A 277, 524
Buchler, J.R., 1998, In: Bradley P.A., Guzik J.A. (eds.) A Half-Century of Stellar Pulsation Interpretations. ASP Conference Series Vol. 135, p. 220
Butler R.P., 1993, ApJ 415, 323
Chadid M., Gillet D., 1997, A&A 315, 480
Fokin A.B., Gillet D., 1997, A&A 325, 1013
Fokin A.B., Gillet D., Breitfellner M.G., 1996, A&A 307, 503 (FGB)
Fokin A.B., Gillet D., Chadid, 1998, A&A in press
Gillet D., Debiève J.F., Fokin A.B., Mazauric S., 1998, A&A 332, 235
Gillet D., Burnage R., Kohler D., et al., 1994, A&AS 108, 181
Sasselov D.D., Lester J.B., 1994, ApJ 423, 795
Xiong D.R., Cheng Q.L., Deng L., 1998, ApJ 500, 449